*Daute Fratta*[1] *and J. Carlos Santamarina*[1]

# Wave Propagation in Soils: Multi-Mode, Wide-Band Testing in a Waveguide Device

---

**REFERENCE:** Fratta, D. and Santamarina, J. C., **"Wave Propagation in Soils: Multi-Mode, Wide-Band Testing in a Waveguide Device,"** *Geotechnical Testing Journal,* GTJODJ, Vol. 19, No. 2, June 1996, pp. 130–140.

**ABSTRACT:** This paper presents the development of a waveguide device and the corresponding processing methodology to study wave propagation in particulate materials. Its main advantages are: the cancellation of biasing transfer functions (e.g., transducer, coupling, and electronics); the determination of both velocity and attenuation in a wide frequency range; the evaluation of torsional, flexural, and longitudinal propagation modes; and the computation of field propagation parameters from laboratory multi-mode data. Fundamentals of signal processing are reviewed, followed by a discussion of design considerations including boundary effects and geometric dispersion. Typical results are presented.

**KEYWORDS:** wave propagation, signal processing, material testing, phase velocity, attenuation, damping

## Introduction—Laboratory Studies of Propagation

The study of wave propagation in discrete media can be traced back to the work by Newton on sound propagation in air. Further developments in the nineteenth century included adequate models of dispersion whereby velocity and attenuation vary with frequency. At the beginning of this century, still in the pre-electronic era, B. Hopkinson studied stress pulses in solids in which the wavelength was much larger than the diameter of the bar. Later, R. Davies created an electronic version of Hopkinson's bar and overcame some of the early problems, allowing for the study of shorter wavelengths and the shape of the pressure-time curve (Kolsky 1963).

The propagation of mechanical waves in uncemented particulate media is still under research. Extensive data are available on wave velocity, primarily at a single frequency. However, the information on attenuation is limited because of measurement difficulties, e.g., transducer-media coupling, and complexity in data interpretation, e.g., the prevailing effect of geometric attenuation. Current research issues address the understanding of wave propagation from a micro-mechanics perspective, the relative contribution of electrostatic forces in fine particles of high specific surface like clays, the effect of creep at contacts, and the role of cementation due to salt precipitation or the formation of silicates (Fam and Santamarina 1995).

The adequate understanding of wave propagation in particulate materials opens avenues to significant potential applications in material characterization and process monitoring in civil engineering systems, particularly those in the near surface. The unique combination of inversion mathematics with wave propagation, for example, allows for the tomographic imaging of field parameters as a function of boundary measurements of wave propagation. The implications are prominent, such as monitoring the migration of contaminants, evaluating the evolution of bentonite-cement slurry walls, and assessing the change in the state of stress in varied geotechnical systems including foundations, retaining walls, and slopes (Santamarina and Potts 1994).

Typical devices used to measure wave velocity and attenuation in geotechnical engineering are classified according to the type of excitation: pulse testing (Stokoe and Woods 1972), steady-state resonance (Hardin and Drnevich 1972), and free vibration methods (Richart et al. 1970). Pulse methods are used both in the laboratory and in the field; however, coupling problems between sensors and the medium and geometric spreading invalidate the use of this type of excitation for attenuation measurements in most cases. In resonant testing, damping and velocity are determined only for a narrow frequency band around resonance. Likewise, both parameters are determined only at the frequency of the first mode in free vibration methods.

The purpose of this study was to develop a simple device to measure frequency-dependent velocity and attenuation in particulate materials. This paper starts with a review of velocity and attenuation for different propagation modes. Then, relevant signal-processing concepts are summarized. Finally, the design of the waveguide device and the processing algorithm are presented followed by typical results.

## Velocity and Attenuation—Propagation Mode

Wave propagation in particulate media can be described by frequency-dependent velocity and attenuation. Velocity and attenuation vary for different modes of propagation. Velocity depends on the elastic and inertial properties of the medium. In nondispersive elastic media, the P-wave (infinite space), longitudinal wave (longitudinal—rod), S-wave, and Rayleigh wave velocities are:

---

[1] Graduate student and associate professor, respectively, School of Civil and Environmental Engineering, Georgia Institute of Technology, Atlanta, GA 30332-0355 (formerly at University of Waterloo, Canada).

© 1996 by the American Society for Testing and Materials

www.astm.org
Copyright by ASTM Int'l (all rights reserved); Tue Nov 17 00:02:06 EST 2009
Downloaded/printed by
Georgia Institute of Technology pursuant to License Agreement. No further reproductions authorized.

$$V_P = \sqrt{\frac{M}{\rho}} = V_L\sqrt{\frac{1-\upsilon}{(1+\upsilon)(1-2\upsilon)}} \quad \text{P-wave} \qquad (1)$$

$$V_L = \sqrt{\frac{E}{\rho}} \quad \text{Longitudinal wave} \qquad (2)$$

$$V_S = \sqrt{\frac{G}{\rho}} = V_L\sqrt{\frac{1}{2(1+\upsilon)}} \quad \text{S-wave} \qquad (3)$$

$$V_R = \frac{\kappa_S}{\kappa_R}V_S = \frac{\kappa_S}{\kappa_R}V_L\sqrt{\frac{1}{2(1+\upsilon)}} \quad \text{Rayleigh wave} \qquad (4)$$

where $M$, $E$, and $G$ are the constrained, longitudinal, and shear moduli, $\rho$ is the material density, $\kappa_S = \omega/V_S$, $\kappa_R = \omega/V_R$, and the ratio $\kappa_S/\kappa_R$ is equal to 0.919 for Poisson's ratio $\upsilon = 0.25$. Measured rod values for $V_L$ and $V_S$ can be used to determine Poisson's ratio

$$\upsilon = \frac{1}{2}\left[\frac{V_L}{V_S}\right]^2 - 1 \qquad (5)$$

and to compute the field velocity $V_P$ according to Eq 1.

Amplitude decays as a function of time and distance. Attenuation reflects geometrical spreading, scattering at boundaries, diffraction around voids and inclusions, and material losses due to viscous and hysteretic processes; energy is dissipated in the form of heat and emissions. The two typical cases of geometrical attenuation are (from Green's theorem):

$$\frac{A_2}{A_1} = \frac{r_1}{r_2} \quad \text{for spherical spreading} \qquad (6)$$

$$\frac{A_2}{A_1} = \sqrt{\frac{r_1}{r_2}} \quad \text{for cylindrical spreading} \qquad (7)$$

where amplitudes $A_1$ and $A_2$ are determined at corresponding distances $r_1$ and $r_2$ from the source. Plane waves and 1-D propagation are not subjected to geometrical spreading.

Distributed material losses are modeled as an exponential decay. For measurements conducted at two different locations

$$A_2 = A_1 e^{-\alpha_r(r_2-r_1)} \qquad (8)$$

where $\alpha_r$ is the attenuation coefficient in distance. When measurements are performed at the same location but at different times

$$A(t_2) = A(t_1)e^{-\alpha_t(t_2-t_1)} \qquad (9)$$

where $A(t_1)$ and $A(t_2)$ are the amplitudes at times $t_1$ and $t_2$, respectively, and $\alpha_t$ is the attenuation coefficient in time. The damping coefficient $D$ and the quality factor $Q$ are commonly used instead of $\alpha$. The relationships between these measurements of attenuation under low-loss assumptions follow (Hall and Richart 1963; Johnston and Toksöz 1981):

$$D = \frac{\alpha_r\lambda}{2\pi} \qquad (10)$$

$$D = \frac{\alpha_t T}{2\pi} \qquad (11)$$

$$\frac{1}{Q} = 2D \qquad (12)$$

where $T$ is the period, and $\lambda$ is the wavelength. Winkler and Nur (1979) derived the relationship between the quality factors in isotropic elastic materials for plane P-waves in infinite media, longitudinal waves in rods, shear waves, and bulk compression. These expressions assume low-loss mechanisms. In terms of damping, these relationships are

$$D_P(1-\upsilon)(1-2\upsilon) = D_L(1+\upsilon) - 2D_S\upsilon(2-\upsilon) \qquad (13)$$

$$D_K(1-2\upsilon) = 3D_L - 2D_S(1+\upsilon) \qquad (14)$$

$$D_K(1+\upsilon) = 3D_P(1-\upsilon) - 2D_S(1-2\upsilon) \qquad (15)$$

where $D_P$ is the damping for plane P-waves in infinite media, $D_L$ for longitudinal waves in rods, $D_S$ for shear waves, and $D_K$ for bulk compression. These expressions imply that one of the following relations must be true:

$$D_S > D_L > D_P > D_K \qquad (16)$$

or

$$D_S = D_L = D_P = D_K \qquad (17)$$

or

$$D_S < D_L < D_P < D_K \qquad (18)$$

Equations 13, 14, and 15 can be combined to obtain field attenuation from laboratory measurements of attenuation in the longitudinal and shear modes:

$$\frac{D_P}{D_S} = \frac{\frac{D_L}{D_S}(1+\upsilon) - 2\upsilon(2-\upsilon)}{(1-\upsilon)(1-2\upsilon)} \qquad (19)$$

$$\frac{D_K}{D_S} = \frac{3\frac{D_L}{D_S} - 2(1+\upsilon)}{1-2\upsilon} \qquad (20)$$

These expressions are plotted in Fig. 1 in terms of $D_L/D_S$ for different values of Poisson's ratio. The constraints expressed in Eqs 16, 17, and 18 are readily confirmed in these plots.

## Brief Review of Signal Processing for Propagation Studies

The process of wave-material interaction can be considered as the transformation of an input signal $x(t)$ into an output signal $y(t)$ through the unknown transfer function of the soil mass $h(t)$. The goal of this study is to obtain $h(t)$ knowing $x(t)$ and $y(t)$. Linear time invariance is assumed, meaning that the superposition principle applies (linear behavior is restricted to low strain) and that the system does not change its response during a measurement (Oppenheim and Willsky 1983).

The input and output time series can be represented by a summation of sines and cosines. Using this representation, the signals in the time domain are transformed to the frequency domain without losing information. The Fourier transform is defined as:

$$X(\omega) = \int_{-\infty}^{\infty} x(t)e^{-j\omega t}dt \qquad (21)$$

and its inverse is:

$$x(t) = \int_{-\infty}^{\infty} X(\omega)e^{j\omega t}d\omega \qquad (22)$$

where $\omega$ is the circular frequency. The transformation equation for digital signals of finite lengths is:

$$X(m\Delta\omega) = \frac{T}{N}\sum_{n=0}^{N-1} x(n\Delta t)e^{-jnm/N} \qquad (23)$$

Copyright by ASTM Int'l (all rights reserved); Tue Nov 17 00:02:06 EST 2009
Downloaded/printed by
Georgia Institute of Technology pursuant to License Agreement. No further reproductions authorized.

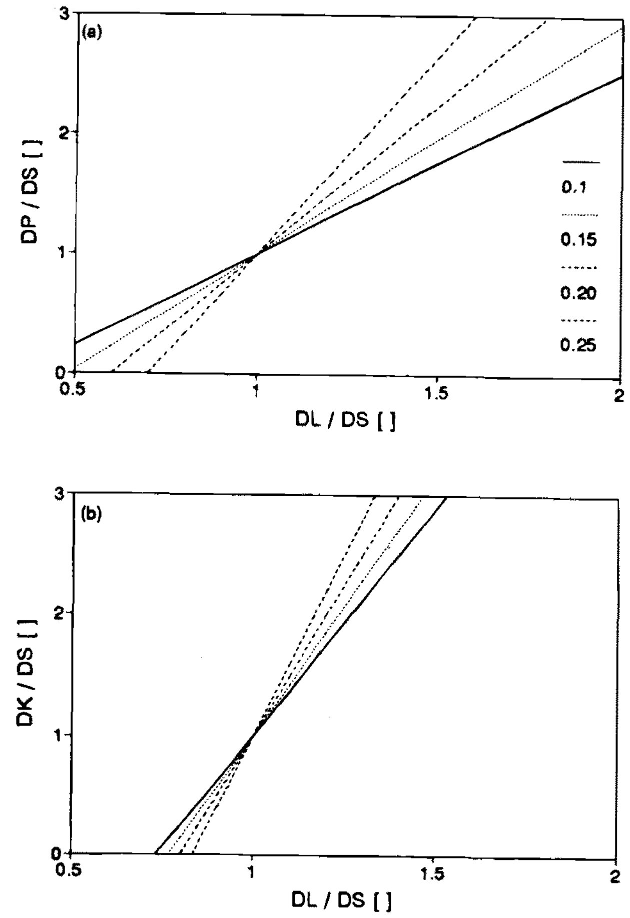

FIG. 1—*Damping in infinite and bounded media: Computation of field damping from laboratory measurements for different Poisson's ratios:* (a) *damping for P-waves;* (b) *damping for bulk compression.*

TABLE 1—*Summary of the functions used in signal processing.*

| | Ideal Signal | Noisy Signal |
|---|---|---|
| Time Domain | | |
| Input Signal | $x(t)$ | $x(t)$ |
| Output Signal | $y(t)$ | $y(t) + s(t)$ |
| Frequency Domain | | |
| Input Signal | $X(\omega)$ | $X(\omega)$ |
| Output Signal | $Y(\omega)$ | $Y(\omega) + S(\omega)$ |
| Fourier Transform (FFT) | $X(\omega) = Re\ X(\omega) + Im\ X(\omega)$ | |
| Complex Conjugate | $X^*(\omega) = Re\ X(\omega) - Im\ X(\omega)$ | |
| Power Spectrum Density | $Psd(\omega) = (ReX(\omega))^2 + (Im\ Y(\omega))^2$ | |
| Cross Power Spectrum | $G_{yx} = Y(\omega)X^*(\omega)$ | |
| Average Cross Power Spectrum[a] | $\overline{G_{yx}} = \overline{Y(\omega)X^*(\omega)}$ | |
| Cross Correlation | $C_{yx} = FFT^{-1}(G_{yx})$ | |
| Transfer Function[a] | $H(\omega) = \frac{Y(\omega)}{X(\omega)}$ | $H(\omega) = \frac{\overline{G_{yx}}}{\overline{G_{xx}}}$ |
| Phase Shift | $\varphi(\omega) = \tan^{-1}\left[\frac{ImH(\omega)}{ReH(\omega)}\right]$ | |
| Modulus | $\lvert H(\omega)\rvert = \sqrt{(ReH(\omega))^2 + (ImH(\omega))^2}$ | |
| Coherence Function[a] | n/a | $\gamma^2(\omega) = \frac{\overline{G_{yx}}\,\overline{G^*_{yx}}}{\overline{G_{xx}}\,\overline{G_{yy}}}$ |
| Signal-to-Noise Ratio | n/a | $SNR(\omega) = \frac{\gamma^2(\omega)}{1 - \gamma^2(\omega)}$ |

[a] The bar over functions means average of multiple similarly measured signals.

where $N$ is the number of points in the time series, $\Delta t$ is the sampling interval, $\Delta\omega$ is the frequency interval, and $m$ and $n$ are integers. Signal processing in the frequency domain permits computing phase and amplitude changes between input and output signals as a function of frequency. Table 1 summarizes functions and operations needed for noiseless and noisy signals. In the case of noisy signals, averaging results in noise cancellation. The signal-to-noise ratio function evaluates the relative strength of the signal with respect to noise. The coherence function indicates how much of the output can be caused by the input (Otnes and Enochson 1978; Hewlett-Packard 1991).

## Waveguide Device (PDC)

The test device is shown in Fig. 2*a*. It consists of a long cylindrical specimen that acts as a waveguide to the propagating signal. The geometry of the specimen is $L \approx 1.6$ m long and $d = 0.10$ m in diameter. The top cap is made of aluminum (diameter $d = 0.10$ m and thickness $th = 0.012$ m). The specimen rests on a steel rod $L_S = 0.58$ m long and $d = 0.10$ m in diameter. The steel rod is attached to a steel base 0.01 m thick and 0.55 m wide. The particulate material under test is contained within a latex membrane, and confining pressure is applied by internal vacuum or external pressure.

Pulse testing the specimen as a waveguide and first-mode vibration testing are possible with such a device. In pulse testing, the signal and its multiple reflections are monitored by a single sensor. One-dimensional propagation avoids geometrical spreading, and one-sensor monitoring permits canceling the transfer function of the transducer and electronics (demonstrated later in the text). Similar types of self-correcting measurements have been used elsewhere (Achenbach et al. 1992). Phase velocity and attenuation can be determined for longitudinal, torsional-shear, and flexural modes of propagation.

### *First-Mode Testing*

In first-mode free-vibration testing, a quasi-static displacement or rotation is imposed on the specimen. Then the specimen is released and the amplitude of oscillation is measured with time. First-mode longitudinal excitation is difficult to generate because motion rapidly changes into flexural vibration due to the high slenderness of the specimen.

Flexural waves are dispersive for all frequencies. For long wavelengths, the dispersion relation can be approximated as $V_L^{Flex} = \pi V_L d/(2\lambda)$ (Kolsky 1963), where $V_L^{Flex}$ is the longitudinal wave

Copyright by ASTM Int'l (all rights reserved); Tue Nov 17 00:02:06 EST 2009
Downloaded/printed by
Georgia Institute of Technology pursuant to License Agreement. No further reproductions authorized.

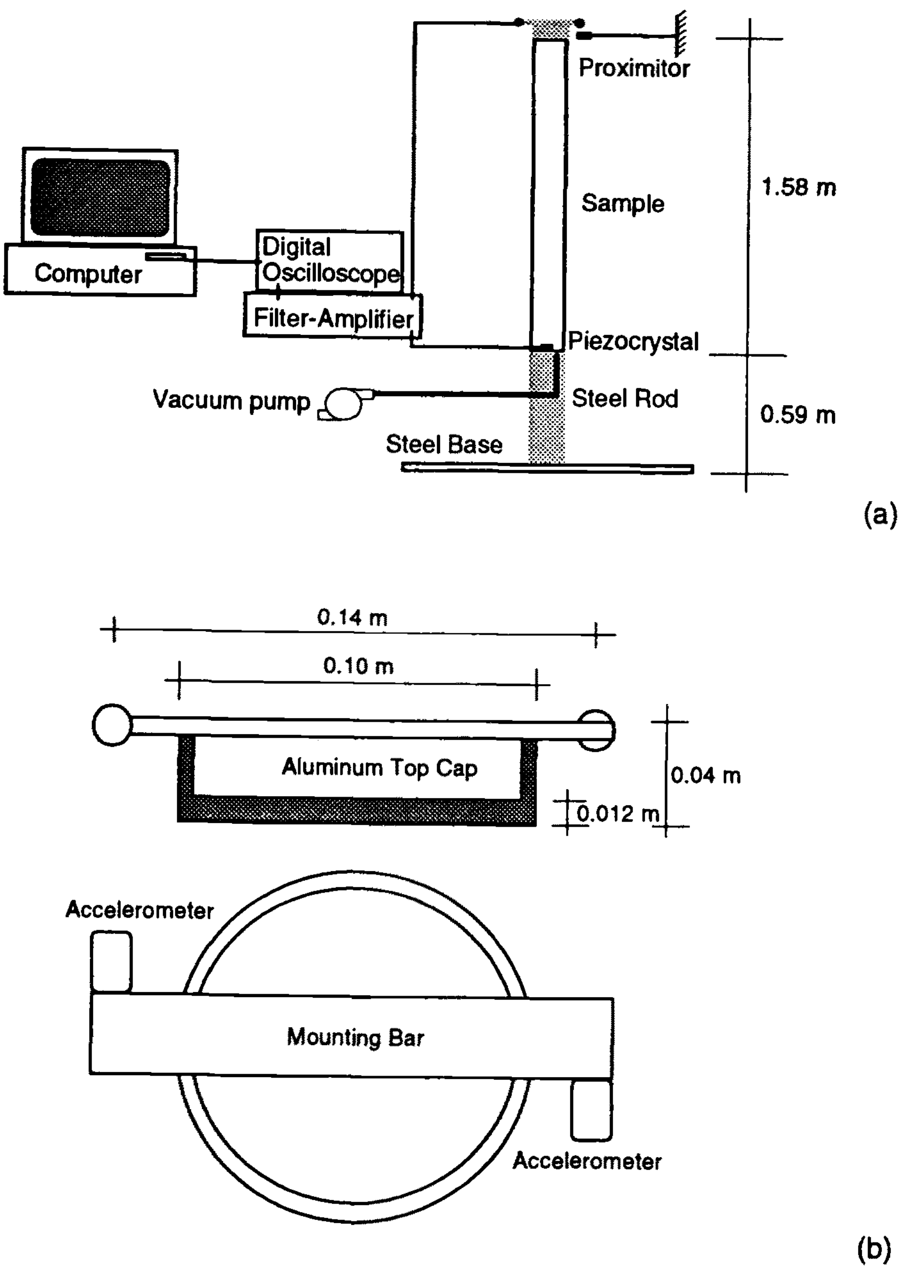

FIG. 2—*Device and experimental setup:* (a) *schematic diagram of general device and instrumentation;* (b) *detail of top cap for torsional vibration monitoring.*

velocity in flexural excitation. Our approach was to use energy principles to determine the first mode of a cantilever beam of constant stiffness considering only flexural energy (Jacobsen and Ayre 1958). The solution is in terms of $E$ and $\rho$; thus, it is used to compute the longitudinal wave velocity from flexural excitation

$$V_L = \frac{2\pi f_F L^2}{0.88\, d} \qquad (24)$$

where $d$ is the diameter of the specimen. For nondispersive shear waves, energy principles are used to compute the shear wave velocity directly from the first mode torsional excitation. The assumed deformed shape of the column is a quarter of sine wave.

$$V_S = 4 f_T L \qquad (25)$$

Equations 24 and 25 apply for fixed-free conditions and massless cap. More accurate equations were derived to take the cap into consideration; however, the effect is small for the first mode of this device.

On the other hand, attenuation in time is computed from the logarithmic decrement of peak amplitudes

$$\alpha_t = \frac{1}{(j-i)T} \ln \frac{A(iT)}{A(jT)} \qquad (26)$$

where $i$ and $j$ are the correlative number of selected peaks and $A$ is amplitude. In this study $\alpha_t$ was obtained by fitting Eq 26 to the peaks of the measured signal.

### *Pulse Testing: Velocity*

Velocity dispersion can be assessed by: the "π-point" phase comparison method, the phase spectrum approach, and the amplitude spectrum approach (Sachse and Pao 1978; Pialucha et al.

Copyright by ASTM Int'l (all rights reserved); Tue Nov 17 00:02:06 EST 2009
Downloaded/printed by
Georgia Institute of Technology pursuant to License Agreement. No further reproductions authorized.

1989). The $\pi$-point method requires changing the propagation distance of a monochromatic wave within the specimen until a $\pi$-phase change is obtained in the received signal. This method can also be implemented by changing the excitation frequency and measuring the phase change between input and output at fixed points. This method is tedious and difficult to implement in solids (Sachse and Pao 1978). In the phase spectrum approach, phase velocity is obtained from two separate measurements in transmission or echo pulse. The method determines the phase spectrum of the input and output signals, and the phase velocity is calculated from the difference of these spectra $\varphi(\omega)$,

$$V^{ph}(\omega) = \frac{\omega L}{\varphi(\omega)} \tag{27}$$

This method requires the discrimination of the different reflections in echo mode. Alternatively, the amplitude spectrum approach is preferred when reflections can not be discriminated (Pialucha et al. 1989).

The phase spectrum approach is used in this work, but modified to account for low signal-to-noise ratios at very low frequencies (unexpected jumps in the saw-tooth phase diagram). The method can be summarized as follows:

1. Determine the change in phase between two consecutive reflections $a(t)$ and $b(t)$ from the transfer function $H(\omega)$ that relates $A(\omega)$ and $B(\omega)$:

$$\varphi(\omega) = \frac{Im(H(\omega))}{Re(H(\omega))} \tag{28}$$

2. Unwrap phase changes by adding $2\pi$ at every phase jump in the phase-versus-frequency plot.
3. Curve fit the nondispersive low-frequency range and determine the zero-frequency intercept $\phi_0$.
4. Subtract $\phi_0$ from the unwrapped phase to obtain the corrected phase $\varphi'(\omega)$.
5. Compute phase velocity for each frequency $V^{ph}(\omega)$ according to Eq 27 with the corrected phase $\varphi'(\omega)$.

It can be shown that the coherence function remains at $\approx 1.0$ without major valleys in the region where this analysis is acceptable.

*Correction for Geometry Dispersion*—The propagation of longitudinal waves is dispersive in rods even if the material is nondispersive. The velocity for longitudinal waves computed in Eq 2 presumes that the cross section of the rod remains plane during the propagation of the wave. This is valid for low frequencies and implies that central and peripheral elements within the rod deform in three dimensions as unconstrained bodies. As the frequency increases, inertial forces become important: central elements in the rod are effectively constrained and forced to deform only in the longitudinal direction (stiffness $M$ and velocity $V_P$—Eq 1), while peripheral elements are still unconstrained without radial normal stress or shear component, $\sigma_r = 0$ and $\tau_{rz} = 0$ (stiffness $E$ and velocity $V_L$). Thus, the wave front curves (note the Rayleigh-type motion of peripheral elements). When the wavelength approaches the radius of an infinitely long rod, the velocity of propagation is the Rayleigh wave velocity. The frequency dependency of the inertial component explains the dispersive nature of propagation. This qualitative analysis is captured in Rayleigh's approximate solution, which fits well Pochhammer's close form solution for long wavelengths, $d/(2\lambda) < 0.15$. The Rayleigh equation is:

$$\frac{V_{ph}}{V_L} = 1 - \pi^2 \upsilon^2 \left(\frac{d}{2\lambda}\right)^2 \tag{29}$$

where $V_L$ is the phase velocity for infinite wavelength. Torsional waves do not present dispersion in the first mode of vibration, i.e., each section rotates as a unit about its center (Kolsky 1963).

*Pulse Testing: Attenuation*

Digitized signals are modified time series of the wave that arrived at the transducer. Alterations are imposed by the coupling of the transducer to the soil mass and by the response of the transducer and the peripheral electronic devices used in the measurements (e.g., cables, filters, amplifiers, A/D converter, etc.). Given an input signal $x(t)$ with Fourier transform $X(\omega)$, the measured signal is $X_1(\omega) = X(\omega)H_x(\omega)$, where $H_x(\omega)$ is the system transfer function at the input. The output signal $y(t)$ in the frequency domain is $Y(\omega) = e^{(-\alpha_r(\omega) \cdot 2L)} e^{(-j\Delta\varphi(\omega))} X(\omega)$, which is the input signal but attenuated and time shifted through the specimen. The measured signal $Y_1(\omega)$ is also affected by the installation and peripherals, hence $Y_1(\omega) = e^{(-\alpha_r(\omega) \cdot 2L)} e^{(-j\Delta\varphi(\omega))} X(\omega) H_y(\omega)$, where $H_y(\omega)$ is the system transfer function at the output. The material transfer function is:

$$H(\omega) = \frac{Y_1(\omega)}{X_1(\omega)} = \frac{e^{(-\alpha_r(\omega) \cdot 2L)} e^{-j\Delta\varphi(\omega)} X(\omega) H_y(\omega)}{X(\omega) H_x(\omega)} \tag{30}$$

and the modulus is:

$$|H(\omega)| = \frac{|Y_1(\omega)|}{|X_1(\omega)|} = \left|\frac{H_y(\omega)}{H_x(\omega)}\right| e^{-\alpha_t(\omega)L} \tag{31}$$

When multiple reflections are measured with a single sensor, the system transfer functions $H_x(\omega)$ and $H_y(\omega)$ are one and the same. Finally, attenuation in distance $\alpha_r(\omega)$ can be determined as (see also Kline 1984):

$$\alpha_r(\omega) = \frac{1}{2L} \ln \left|\frac{X_1(\omega)}{Y_1(\omega)}\right| \tag{32}$$

*Correction for Boundaries*—The device designed for these tests resembles free-fixed boundary conditions. The high-impedance boundary is modeled with the steel rod and steel base plate to maximize the impedance mismatch. The free-end low-impedance boundary at the top of the specimen was approximated using the thin aluminum cap (see Fig. 2).

The problem of transmission and reflection in three media was solved by evaluating these boundary conditions. The frequency-dependent coefficient of reflection for the lower steel boundary is:

$$c(\omega) = \frac{-\left(1 - \frac{z_1}{z_2}\right)\left(1 + \frac{z_3}{z_2}\right) + \left(1 + \frac{z_1}{z_2}\right)\left(1 - \frac{z_3}{z_2}\right) e^{j(-2\kappa_2 L_S)}}{\left(1 + \frac{z_1}{z_2}\right)\left(1 + \frac{z_3}{z_2}\right) - \left(1 - \frac{z_1}{z_2}\right)\left(1 - \frac{z_3}{z_2}\right) e^{j(-2\kappa_2 L_S)}} \tag{33}$$

where $z_1$, $z_2$, and $z_3$ are the impedances of the specimen, steel, and floor, $\kappa_2$ is the wave number in the steel rod, and $L_S$ is

Copyright by ASTM Int'l (all rights reserved); Tue Nov 17 00:02:06 EST 2009
Downloaded/printed by
Georgia Institute of Technology pursuant to License Agreement. No further reproductions authorized.

the length of the steel rod. Figure 3 shows the modulus of the reflection coefficient versus frequency for a typical soil impedance ($z_1$ = 0.7 GPa·s/m). The impedance of the floor was varied from $z_3$ = 4 to 8 GPa·s/m. For frequencies $f > 1000$ Hz, the reflection coefficient is almost independent of the floor impedance $z_3$, i.e., the impedance of the third medium. Corrections in this study were done considering the impedance of the floor $z_3$ = 6 GPa·s/m.

The frequency-dependent reflection coefficient $c(\omega)$ is taken into consideration in the evaluation of the attenuation coefficient $\alpha_r$ by modifying Eq 32. It can be shown that

$$\alpha_r(\omega) = \frac{1}{2nL}\ln\left|\frac{X_1(\omega)c(\omega)^n}{Y_1(\omega)}\right| \qquad (34)$$

where $n$ is the number of reflections between the input signal $x(t)$ and the output signal $y(t)$. Contrary to the lower boundary, the upper free boundary changes its response to the fixed boundary at high frequencies (approximately 40 kHz).

## Results and Analyses

Results for a multi-propagation mode test are presented in this section. The selected soil was Barco sand ($e_{min}$ = 0.5, $e_{max}$ = 0.74, $D_{10}$ = 0.31 mm, $D_{60}$ = 0.45 mm). The specimen was prepared by the dry pluviation method, raining the sand inside the split mold with the rubber membrane. Additional energy was applied by lightly tapping the sides of the split mold. The final dimensions of the specimen were $L$ = 1.58 m length, diameter $D$ = 0.10 m, unit weight $\gamma$ = 16.7 kN/m$^3$, and void ratio $e$ = 0.55. The specimen was confined by applying negative pore pressure with a vacuum pump. There was a stress gradient throughout the specimen, yet its effect on velocity was less than the error in standard travel time measurement procedures.

Three different transducers were used to capture signals: piezocrystals, accelerometers (Columbia Research model 8402), and a proximitor (Bently Nevada 7200). The sampling rate in the digital storage oscilloscope (Rapid System 2000) was selected in accordance with the Nyquist criterion to adequately capture frequencies of interest. Anti-aliasing filtering and amplification (Krohn Hite 3944) were also used. Stored signals were processed using a signal processing software and computation sheets prepared in MathCad.

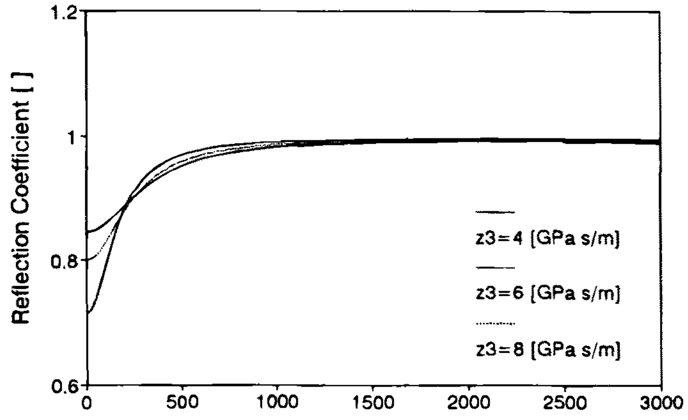

FIG. 3—*Reflection coefficient in three media. Comparison for three different floor impedances,* $z_3$ = *4, 6, and 8 GPa·s/m (soil impedance* $z_1$ = *0.7 GPa·s/m; steel rod impedance* $z_2$ = *40 GPa·s/m).*

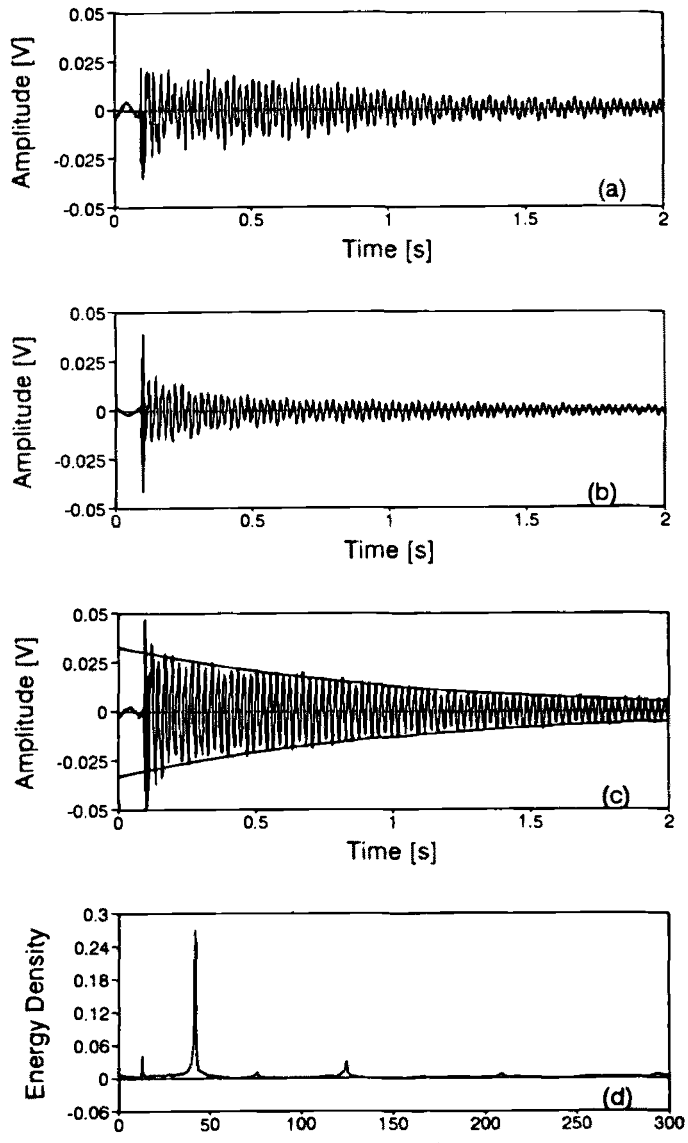

FIG. 4—*First-mode torsional excitation:* (a) *signal from Accelerometer A;* (b) *signal from accelerometer B;* (c) *addition of responses A and B and computed exponential decay;* (d) *power spectral density of combined signal.*

### *First-Mode Results*

First-mode testing was performed by applying a quasi-static deformation on the top of the specimen and suddenly releasing it. Torsional and flexural waves were produced by applying torsional or bending moments, respectively. Because of the slenderness of the specimen and the free boundary condition at the top of the specimen, the system had a great tendency to convert energy into the flexural mode regardless of the type of excitation. Two measurement "tricks" facilitated monitoring the torsional mode. First, accelerometers were used to enhance higher frequency components acting as progressive high-pass filters (the resonant frequency of the torsional mode was significantly higher than the frequency of the first flexural mode—Table 2). Second, two accelerometers were mounted diametrically opposed; signals were combined to cancel the displacement component produced by the flexural mode and to enhance the rotational component correspond-

Copyright by ASTM Int'l (all rights reserved); Tue Nov 17 00:02:06 EST 2009
Downloaded/printed by
Georgia Institute of Technology pursuant to License Agreement. No further reproductions authorized.

TABLE 2—*Summary of results.*

| Mode | Propagation | Velocity | Attenuation |
|---|---|---|---|
| First Mode | Flexural<br>($\epsilon = 1.2 \cdot 10^{-4}$) | $V_L = 392.1$ m/s<br>(at 2.20 Hz) | $\alpha_t = 0.05\ \text{s}^{-1}$<br>$D_F = 0.0036$ |
| | Torsional<br>($\gamma = 3.7 \cdot 10^{-6}$) | $V_S = 264.2$ m/s<br>(at 41.8 Hz) | $\alpha_t = 0.94\ \text{s}^{-1}$<br>$D_S = 0.0040$ |
| Pulse Testing | Torsional<br>($\gamma = 1.0 \cdot 10^{-5}$) | $V_S^{CC} = 261.2$ m/s<br>$V_S^{ph} \approx 263$ m/s (constant) | $\alpha_S = 0.13\ \text{m}^{-1}$ (at 400 Hz)<br>$D_S^{PSD} = 0.0083$<br>$D_S^{TS} = 0.0068$ |
| | Longitudinal<br>($\epsilon = 7.7 \cdot 10^{-7}$) | $V_L^{CC} = 392.1$ m/s<br>$V_L^{ph} \approx 414-370$ m/s(variable) | $\alpha_L = 0.10\ \text{m}^{-1}$ (at 1000 Hz)<br>$D_L^{PSD} = 0.0040$<br>$D_L^{TS} = 0.0041$ |

$V^{CC}$ = calculated with the travel time from cross correlation.
$V^{ph}$ = phase velocity.
$D^{PSD}$ = obtained from power spectral densities in third and fourth reflections.
$D^{TS}$ = obtained from curve-fitting late peaks in pulse testing (see Fig. 6).

ing to the torsional mode. Figure 2*b* shows the mounting of accelerometers on the bar attached to the aluminum cap.

Figure 4 presents the two time series obtained with the accelerometers, the combined signal, and the power spectral density. The measured central frequency is 41.8 Hz. The corresponding shear wave velocity computed with Eq 25 is $V_S = 264.2$ m/s. Attenuation $\alpha_L$ is obtained from the logarithmic decrement by fitting the exponential function to the series of peak amplitudes. Results are summarized in Table 2.

The first-mode flexural vibration occurs at low frequency and was monitored with a proximitor. It was mounted on an auxiliary frame to measure the displacements of the top of the specimen. Figure 5 presents the series obtained from the proximitor, the fitted decay function, and the power spectral density. The measured central frequency is 2.20 Hz. The estimated longitudinal velocity according to Eq 24 is $V_L^{\text{Flex}} = 392.1$ m/s. Results and average strain levels are summarized in Table 2.

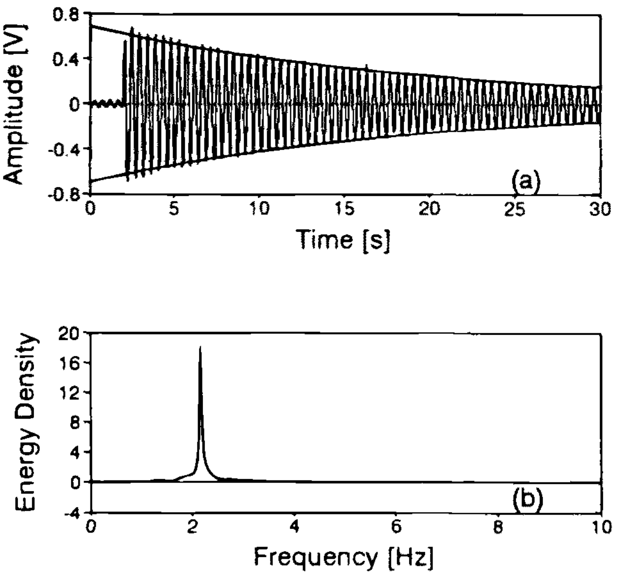

FIG. 5—*First-mode flexural excitation:* (a) *signal from proximitor and computed exponential decay;* (b) *power spectral density of signal.*

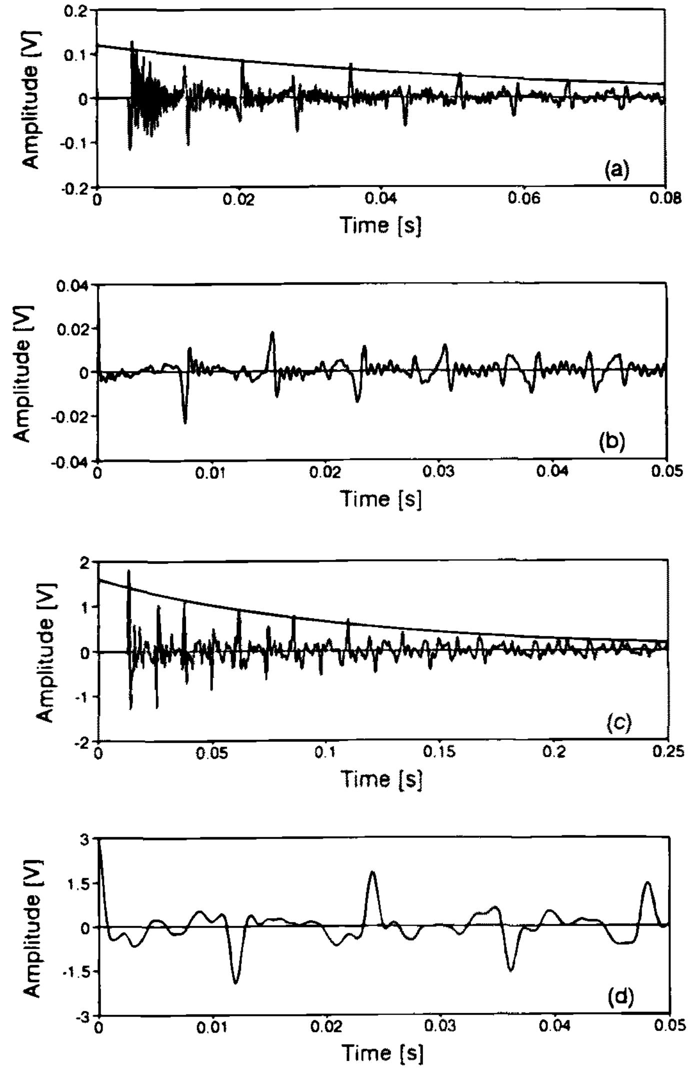

FIG. 6—*Pulse testing—velocity:* (a) *longitudinal excitation: direct signal and reflections;* (b) *longitudinal excitation: autocorrelation;* (c) *torsional excitation: direct signal and reflections;* (d) *torsional excitation: autocorrelation.*

Copyright by ASTM Int'l (all rights reserved); Tue Nov 17 00:02:06 EST 2009
Downloaded/printed by
Georgia Institute of Technology pursuant to License Agreement. No further reproductions authorized.

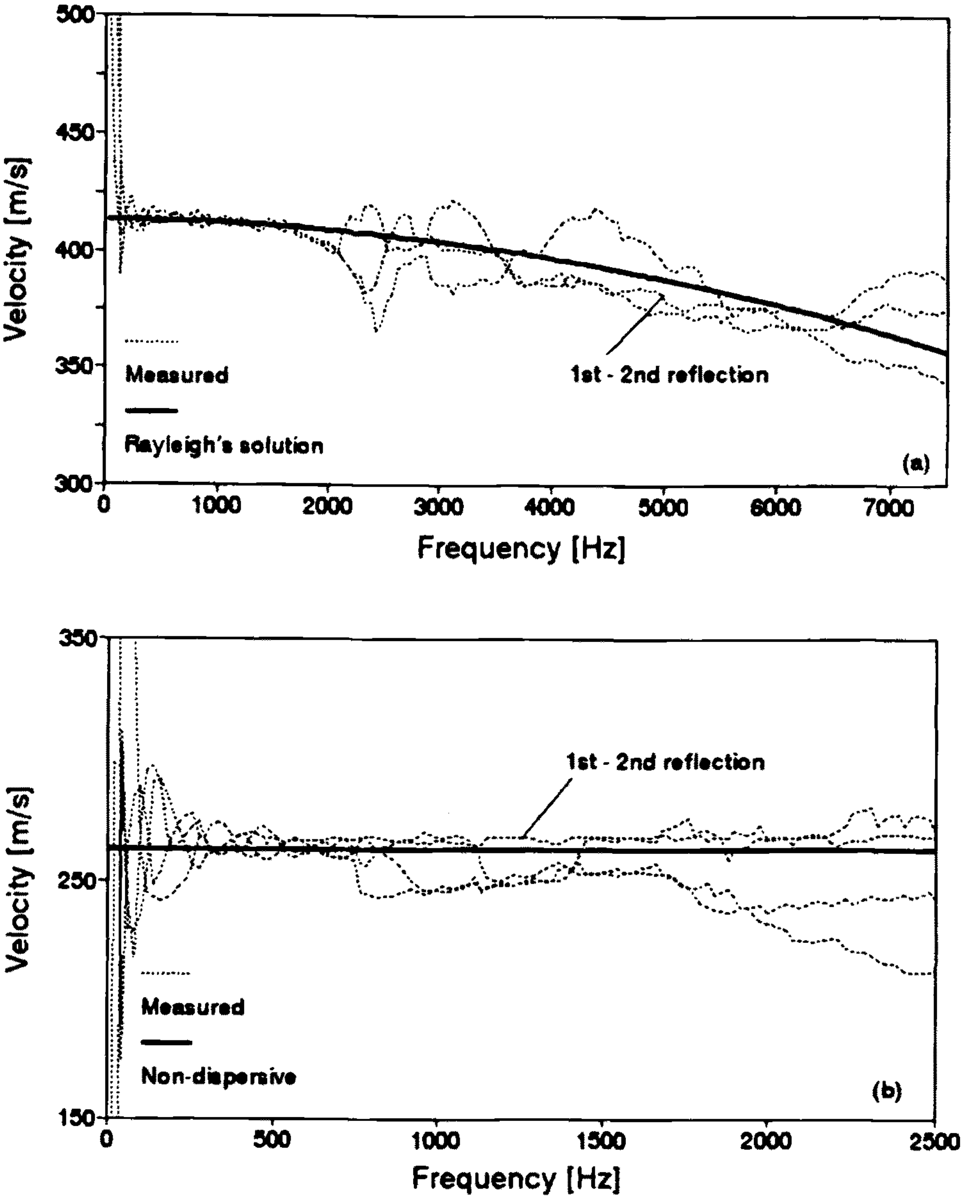

FIG. 7—*Unaveraged phase velocity computed from different reflections:* (a) *longitudinal phase velocity and Rayleigh's approximate solution;* (b) *torsional phase velocity—no dispersion (note: first and second reflections present better signal-to-noise ratios in a wider frequency band).*

*Pulse Testing—Results*

Pulses were produced by free-fall impact. Frequency content, energy, and duration were controlled by varying the height, changing the mass, using different materials for the falling sphere, and by placing "cushions" at the place of the impact.

Longitudinal pulses were monitored with a single piezoelectric crystal mounted horizontally on the lower boundary at the center of the steel rod. Torsional pulses were monitored with the accelerometers mounted on the top cap. In both cases, signal processing was based on the methodology described above for one transducer and multiple reflections.

Figure 6 shows typical longitudinal wave (Fig. 6*a*) and shear wave (Fig. 6*c*) signals and their corresponding autocorrelations (Figs. 6*b* and 6*d*). The change in phase between consecutive reflections due to the free boundary condition at the top is readily seen. Figures 6*a* and 6*c* also present the fitted exponential decay of reflections peaks. The attenuation computed in this case is representative of the central frequency.

Figure 7 presents unaveraged phase velocity plots computed for several reflections in longitudinal and torsional excitation. In each case, the frequency range of the velocity spectrum is conditioned by the signal-to-noise ratio (e.g., see high scatter at very low and high frequencies). The dispersion in the longitudinal phase velocity fits well the theoretical solution given by Rayleigh. The torsional phase velocity presents no dispersion in agreement with theory. These results confirm that the dry sand is nondispersive within the frequency range valid for this analysis.

Poisson's ratio is computed with Eq 5, using $V_S$ and $V_L$ corresponding to the travel time determined with the cross-correlation function (group velocity—energy). The computed value is $\nu = 0.13$.

The frequency-dependent attenuation of longitudinal waves is computed taking into consideration the frequency-dependent reflection of the lower boundary (Eqs 32 and 34). Figure 8 presents results corresponding to the longitudinal excitation. Figure 8*a* shows attenuation values obtained by averaging results values from

Copyright by ASTM Int'l (all rights reserved); Tue Nov 17 00:02:06 EST 2009
Downloaded/printed by
Georgia Institute of Technology pursuant to License Agreement. No further reproductions authorized.

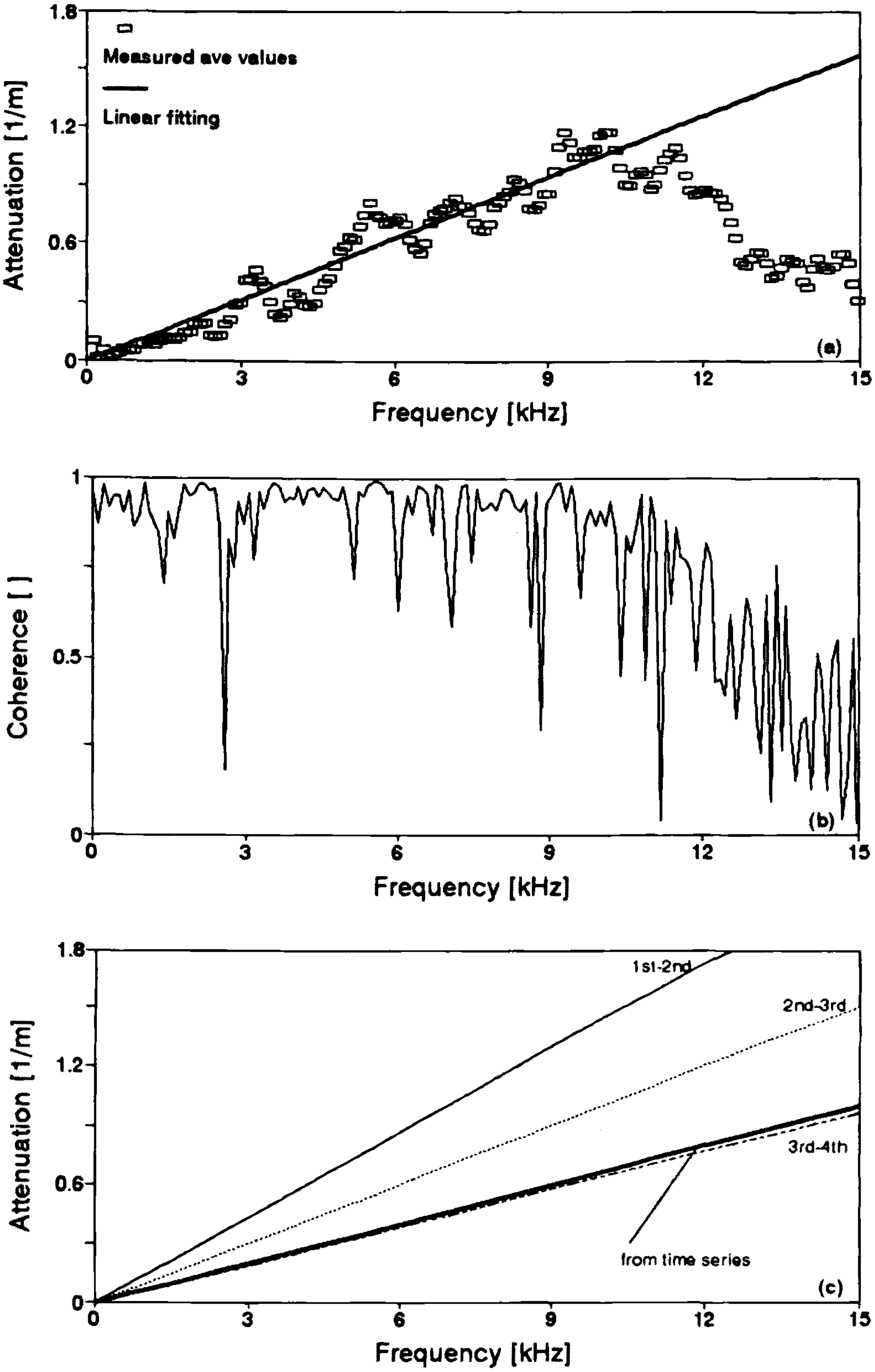

FIG. 8—*Longitudinal pulse testing—attenuation:* (a) *averaged attenuation from five signals and linear regression;* (b) *coherence;* (c) *variation of attenuation with reflection and attenuation obtained from fitting tail peaks in Fig.* 6a.

five reflected signals. Assuming constant damping $D(\omega)$, the linear regression of $\alpha_1(\omega)$ versus $\omega$ is computed in the region where coherence remains close to 1.0. Attenuation deviates from the linear fit when coherence drops at high frequencies ($f > \approx 10$ kHz; Fig. 8*b*). Figure 8*c* presents the decrease in computed attenuation when later reflections are considered. This figure also includes the attenuation coefficient calculated by curve fitting the peaks of the time series (Fig. 6*a*). Figure 9 presents similar results for the torsional excitation (Eq 32—uncorrected for reflection loss). The scatter in the measured averaged values at 0.1 and 1.1 kHz (Fig.

Copyright by ASTM Int'l (all rights reserved); Tue Nov 17 00:02:06 EST 2009
Downloaded/printed by
Georgia Institute of Technology pursuant to License Agreement. No further reproductions authorized.

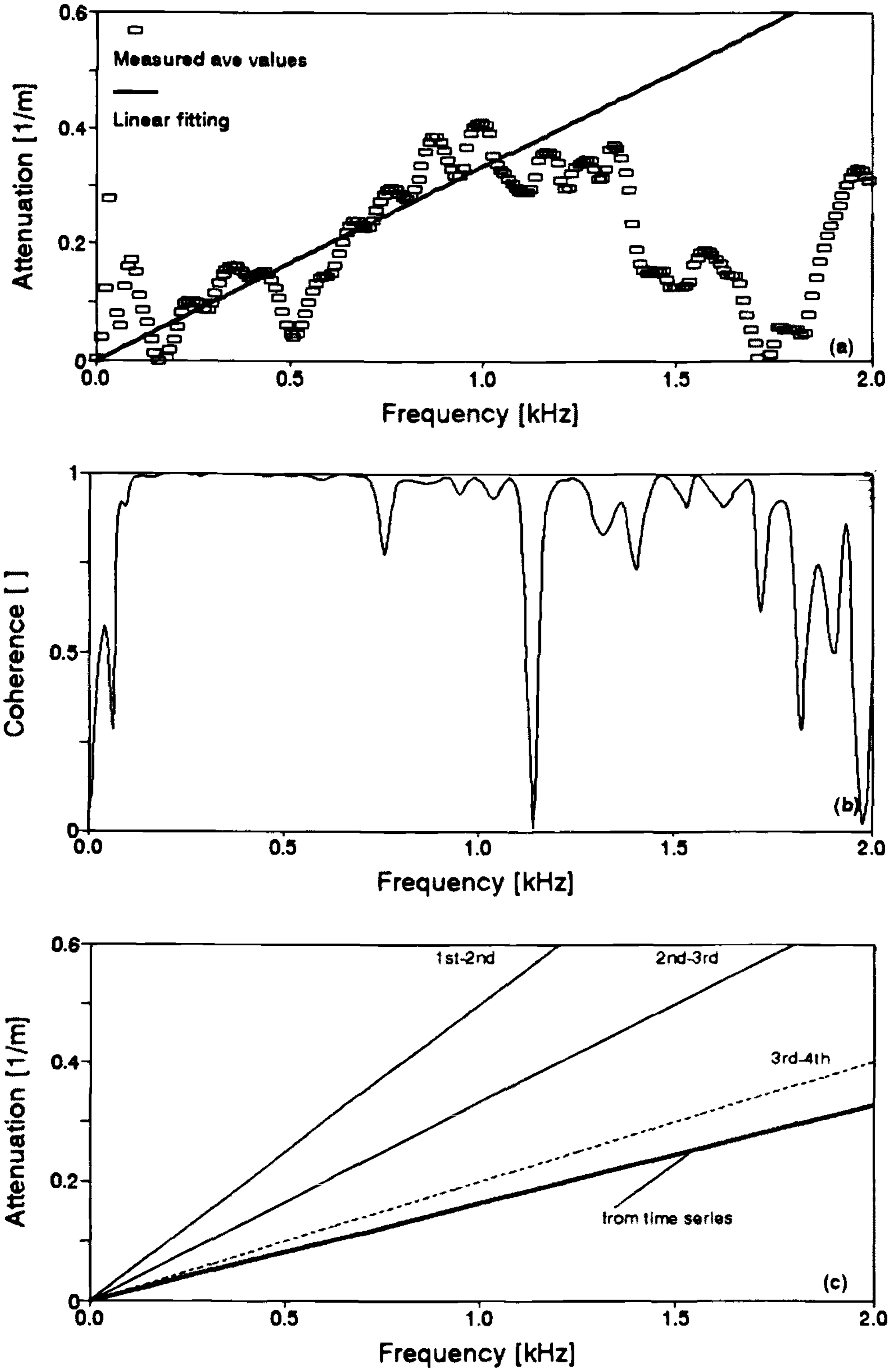

FIG. 9—*Torsional pulse testing—attenuation:* (a) *averaged attenuation from five signals and linear regression;* (b) *coherence;* (c) *variation of attenuation with reflection and attenuation obtained from fitting tail peaks in Fig. 6*c.

Copyright by ASTM Int'l (all rights reserved); Tue Nov 17 00:02:06 EST 2009
Downloaded/printed by
Georgia Institute of Technology pursuant to License Agreement. No further reproductions authorized.

9*a*) coincide with a drop in the coherence level (Fig. 9*b*). Results and estimated average strain levels are summarized in Table 2.

### *Comparison—Field Values*

Velocities computed from torsional first-mode testing are almost identical to those measured in torsional pulse mode (Table 2). These results show consistency between the two modes of testing. The field P-wave velocity can be estimated from Eq 1: for Poisson's $v = 0.13$, $V_P = 1.020\ V_L$. Unless an adequate mechanical model of the system is available, first-mode testing is more prone to bias. In any case, pulse propagation is richer in information.

Damping values for shear wave propagation are similar for first-mode and pulse propagation. The field value for the attenuation of P-waves is computed with Eq 19 (Fig. 1*a*): given $D_L/D_S = 0.64$, $D_P = 0.0025$ ($D_S$ and $D_L$ corresponds to damping values calculated from curve fitting the peaks of pulse time series—see Fig. 6). The computed bulk damping is negative. Winkler and Nur (1979) also computed negative values of $D_K$ for a dry specimen of Massilon Sandstone and argued on the effect of data errors. In our case, the different strain levels compound with the sensitivity of the mapping for $D_L/D_S < 1$, leading to negative values. Other explanations must be explored, such as the foundations of Eqs 13, 14, and 15 and the implications of the linear elastic isotropic assumption made in their derivation. In any case, further analyses must be conducted with realistic numbers of signal stacking to adequately increase the signal-to-noise ratio.

## Conclusions

The proposed waveguide device and test procedure involve multi-mode wave propagation testing to determine velocity and damping. These parameters can be obtained for a wide frequency range using pulse transmission or, for a single frequency, using first-mode vibration and logarithmic decrement analysis.

In pulse transmission, a single sensor is used and multiple reflections are detected. This setup results in the cancellation of the system's transfer function, including the effects of the transducer, the transducer-soil coupling, and the peripheral electronics. Geometry dispersion in bounded media and frequency-dependent reflection at boundaries must be taken into consideration.

Field velocity and damping can be determined from multi-mode laboratory measurements.

### *Acknowledgments*

The authors are grateful to G. Cascante for suggestions and discussions. This research is part of a study on wave-geomedia interaction and applications conducted at the University of Waterloo with support from the Natural Science and Engineering Research Council of Canada, NSERC.

## References

Achenbach, J. D., Komsky, I. N., Lee, Y. C., and Angel, Y. C., 1992, "Self-Calibrating Ultrasonic Technique for Crack Depth Measurement," *Journal of Nondestructive Evaluation*, Vol. 11, No. 2, pp. 103–108.

Fam, M. A. and Santamarina, J. C., 1995, "Study of Geoprocesses with Complementary Mechanical and Electromagnetic Wave Measurements in an Oedometer," *Geotechnical Testing Journal*, ASTM, Vol. 18, No. 3, pp. 307–314.

Hall, J. R. and Richart, F. E., 1963, "Dissipation of Elastic Wave Energy in Granular Soils," *Journal of the Soil Mechanics and Foundation Division, Proceedings of the American Society of Civil Engineers*, Vol. 89, No. SM6, pp. 27–56.

Hardin, B. O. and Drnevich, V. P., 1972, "Shear Modulus and Damping in Soils: Measurement and Parameter Effects," *Journal of the Soil Mechanics and Foundations Division, Proceedings of the American Society of Civil Engineers*, Vol. 98, No. SM6, pp. 603–624.

Hewlett-Packard, 1991, *The Fundamentals of Signal Analysis, Applications Notes 243*, Hewlett-Packard Co. Mississauqa, Canada.

Jacobsen, L. S. and Ayre, R. S., 1958, *Engineering Vibrations with Applications to Structures and Machinery*, McGraw-Hill Book Co., New York.

Johnston, D. H. and Toksöz, M. N., 1981, "Laboratory Measurements of Attenuation," *Seismic Wave Attenuation*, Society of Exploration Geophysicists, Geophysics Reprint Series No. 2, pp. 6–11.

Kline, R. A., 1984, "Measurement of Attenuation and Dispersion Using an Ultrasonic Spectroscopy Technique," *Journal of the Acoustic Society of America*, Vol. 76, No. 2, pp. 498–504.

Kolsky, H., 1963, *Stress Waves in Solids*, Dover Publications, Inc., New York.

Oppenheim, A. J. and Willsky, A. S., 1983, *Signals and Systems*, Prentice-Hall, Inc., Englewood Cliffs, NJ.

Otnes, R. K. and Enochson, L., 1978, *Applied Time Series Analysis*, Vol. 1, John Wiley and Sons, New York.

Pialucha, T., Guyott, C. C., and Cawley, P., 1989, "Amplitude Spectrum Method for the Measurement of Phase Velocity," *Ultrasonics*, Vol. 27, pp. 270–279.

Richart, F. E., Hall, J. R., and Woods, R. D., 1970, *Vibrations of Soils and Foundations*, Prentice Hall, Inc., Englewood Cliffs, NJ.

Sachse, W. and Pao, Y. H., 1978, "On the Determination of Phase and Group Velocities of Dispersive Waves in Solids," *Journal of Applied Physics*, Vol. 49, No. 8, pp. 4320–4327.

Santamarina, J. C. and Potts, B., 1994, "On the Imaging of Stress Changes in Particulate Media—An Experimental Study," *Canadian Geotechnical Journal*, Vol. 31, No. 2, pp. 215–222.

Stokoe, K. H. and Woods, R. D., 1972, "In Situ Shear Wave Velocity by Cross-Hole Method, *Journal of the Soil Mechanics and Foundations Division, Proceedings of the American Society of Civil Engineers*, Vol. 98, No. SM5, pp. 443–459.

Winkler, K. W. and Nur, A., 1979, "Pore Fluids and Seismic Attenuation in Rocks," *Geophysical Research Letters*, Vol. 6, pp. 1–4.

Copyright by ASTM Int'l (all rights reserved); Tue Nov 17 00:02:06 EST 2009
Downloaded/printed by
Georgia Institute of Technology pursuant to License Agreement. No further reproductions authorized.